

DENGUE VIRUS

A T164S mutation in the dengue virus NS1 protein is associated with greater disease severity in mice

Kitti Wing Ki Chan^{1,2}, Satoru Watanabe¹, Jocelyn Y. Jin¹, Julien Pompon^{1,3}, Don Teng⁴, Sylvie Alonso^{2,5}, Dhanasekaran Vijaykrishna^{1,4}, Scott B. Halstead⁶, Jan K. Marzinek⁷, Peter J. Bond⁷, Bo Burla⁸, Federico Torta⁸, Markus R. Wenk⁸, Eng Eong Ooi^{1,2}, Subhash G. Vasudevan^{1,2*}

Copyright © 2019
The Authors, some
rights reserved;
exclusive licensee
American Association
for the Advancement
of Science. No claim
to original U.S.
Government Works

Dengue viruses cause severe and sudden human epidemics worldwide. The secreted form of the nonstructural protein 1 (sNS1) of dengue virus causes vascular leakage, a hallmark of severe dengue disease. Here, we reverse engineered the T164S mutation of NS1, associated with the severity of dengue epidemics in the Americas, into a dengue virus serotype 2 mildly infectious strain. The T164S mutant virus decreased infectious virus production and increased sNS1 production in mammalian cell lines and human peripheral blood mononuclear cells (PBMCs) without affecting viral RNA replication. Gene expression profiling of 268 inflammation-associated human genes revealed up-regulation of genes induced in response to vascular leakage. Infection of the mosquito vector *Aedes aegypti* with the T164S mutant virus resulted in increased viral load in the mosquito midgut and higher sNS1 production compared to wild-type virus infection. Infection of type 1 and 2 interferon receptor-deficient AG129 mice with the T164S mutant virus resulted in severe disease coupled with increased complement activation, tissue inflammation, and more rapid mortality compared to AG129 mice infected with wild-type virus. Molecular dynamics simulations predicted that mutant sNS1 formed stable dimers similar to the wild-type protein, whereas the hexameric mutant sNS1 was predicted to be unstable. Immunoaffinity-purified sNS1 from T164S mutant virus-infected mammalian cells was associated with different lipid classes compared to wild-type sNS1. Treatment of human PBMCs with sNS1 purified from T164S mutant virus resulted in a twofold higher production of proinflammatory cytokines, suggesting a mechanism for how mutant sNS1 may cause more severe dengue disease.

INTRODUCTION

Dengue is a global public health concern caused by four serotypes of the mosquito-borne dengue virus. Several hundred thousand severe dengue cases occur annually with an estimated 40% of the world's population at risk of infection (1). Severe dengue is characterized by hypotension from vasculopathy-associated plasma leakage, internal hemorrhage, and organ dysfunction. Risk of severe dengue appears to be multifactorial and includes host genetic susceptibility factors as well as secondary infection with a dengue virus serotype heterologous to the primary dengue virus infection. More recently, viral factors have also been shown to influence transmission and disease severity in endemic populations. These factors effectively suppress antiviral responses of both human and vector hosts. However, the viral molecular determinants and their mechanistic contributions toward epidemiological and clinical severity remain poorly understood.

In a retrospective study of the 1997 Cuban dengue virus serotype 2 (DENV2) outbreak, a single conservative amino acid substitution in the virus-encoded nonstructural protein 1 (NS1) protein at residue 164 from a threonine (T) to a serine (S) (T164S) was suggested to be

responsible for the enhanced clinical severity among dengue virus cases as the epidemic progressed (2, 3). NS1 is a virus-encoded ~50-kDa glycoprotein that exists in different oligomeric states. It assumes diverse roles in virus replication in the dimeric state. It is also secreted from infected cells in the form of a hexamer with a central lipid-filled channel (4–6). The secreted NS1 (sNS1) lipoprotein interacts directly with endothelial cells or Toll-like receptor 4 (TLR4) on human myeloid-derived cells (7, 8) to activate the complement system (9), which may directly influence vasculopathy and leakage of plasma.

In this study, we combined genomic, virological, immunological, and biochemical analyses to define how the T164S mutation in NS1 influenced replication of dengue virus and disease outcome in cell lines, mosquitoes, and type 1 interferon (IFN)-deficient AG129 mice. We found that the mutation increased sNS1 production coupled with slightly reduced infectious virus production in vitro and in vivo. The elevated sNS1 production by T164S mutant virus induced higher expression of proinflammatory cytokines and complement pathway genes in infected human peripheral blood mononuclear cells (PBMCs). The mutant virus also induced complement-mediated inflammation in mice, resulting in lethality. The lipid load of mutant sNS1 varied potentially, contributing to stability of the hexamer.

RESULTS

The T164S mutation in dengue virus NS1 correlates with increased disease severity

We first examined the conservation of threonine at position 164 (T164) of the dengue virus NS1 protein in the publicly available dengue sequence database (10) and found that T164 was present in >98% of DENV1, DENV3, and DENV4 sequences and 90.8% of DENV2

¹Program in Emerging Infectious Diseases, Duke-NUS Medical School, 8 College Road, Singapore 169857, Singapore. ²Department of Microbiology and Immunology, 5 Science Drive 2, Singapore 117545, Singapore. ³MIVEGEC, UMR IRD 224-CNRS 5290 Université de Montpellier, Montpellier, France. ⁴Biomedicine Discovery Institute and Department of Microbiology, Monash University, Melbourne, Victoria 3800, Australia. ⁵Immunology Programme, Life Sciences Institute, National University of Singapore, Singapore 117456, Singapore. ⁶Department of Preventive Medicine and Biometrics, Uniformed Services University of the Health Sciences, Bethesda, MD 20817, USA. ⁷Bioinformatics Institute (A*STAR), 30 Biopolis St., Singapore 138671, Singapore. ⁸Singapore Lipidomics Incubator (SLING), Department of Biochemistry, Yong Loo Lin School of Medicine, National University of Singapore, Singapore 117597, Singapore.

*Corresponding author Email: subhash.vasudevan@duke-nus.edu.sg

sequences (Fig. 1A). In the three-dimensional (3D) structure of NS1, T164 lies adjacent to the functionally essential “greasy finger” loop amino acid residues 159 to 162 (Fig. 1A) (11). Maximum likelihood phylogenetic analysis of DENV2 sequences (>1600) showed that the T164S substitution in NS1 occurred exclusively within genotype III (Asian/American lineage of dengue virus) (Fig. 1B). The substitution was first observed in a Vietnam isolate (D2/Vietnam/1998) that was an outlier to viruses that were introduced into the Americas (Fig. 1C). Although threonine remains the predominant amino acid at position 164 in NS1 in this clade, the T164S substitution emerged on multiple occasions during severe dengue epidemics in several countries including the United States, Puerto Rico, Venezuela, Cuba, and Peru (Fig. 1C). However, the appearance of T164S in NS1 was only seen in virus samples from severe epidemics caused by the Asian/American virus lineage, suggesting that the T164S substitution is not fixed in the dengue virus population and may be an important marker to identify epidemic-inducing dengue virus strains. We therefore investigated in detail the contribution of the T164S substitution to disease severity using an infectious clone of the DENV2 isolate from Singapore (12, 13).

The T164S mutation increases secretion of sNS1 and reduces infectious virus production in vitro

Given that the T164S mutation is considered to be a conservative change, we first examined the impact of this change on viral RNA replication and infectivity. The T164S mutation was introduced into the DENV2 mildly infectious clone (Fig. 2A) as previously described (13). The in vitro transcribed RNA of wild-type or mutant virus was transfected directly either into the baby hamster kidney 21 (BHK-21) mammalian cell line for assessment of viral replication kinetics or into C6/36 insect cells to generate virions for infection studies. BHK-21 cells transfected with wild-type or T164S viral RNA showed comparable intracellular viral RNA synthesis (Fig. 2B) and extracellular virion-associated RNA (fig. S1A). The infectious titer of the sequence-confirmed T164S mutant virus was 4.5-fold lower ($P = 0.032$) than that of wild-type virus 24 hours after transfection (Fig. 2C, left axis). However, the genome equivalent (GE), which is the ratio of extracellular RNA genome copies (GCs) measured by reverse transcription polymerase chain reaction (RT-PCR) to infectious virus measured by plaque assay [plaque-forming units (pfu)], was similar between wild-type and T164S virus ($\sim 10^4$ GC:1 pfu) in BHK-21 cells (Fig. 2C, right axis) and C6/36 cells (fig. S1B), ruling out the possibility that the T164S virus produced more immature or defective virus particles.

Next, we examined the infection profile of T164S mutant virus in HuH-7 human hepatic cells at a multiplicity of infection (MOI) of 1 or 10, respectively. Analogous to BHK-21 cell transfection, the intracellular viral RNA replication of wild-type and T164S virus was similar regardless of the MOI (Fig. 2D). However, the infectious titer of the T164S virus was lower than that of the wild-type virus 24 hours after infection (MOI 1: 2.1-fold, $P = 0.029$; MOI 10: 1.6-fold, $P = 0.120$) (Fig. 2E). The lower T164S virus titer after infection of HuH-7 cells did not seem to be due to the production of immature or defective virus particles given that the GE and the percentage infection detected by immunofluorescence assay were similar to those of wild-type virus (fig. S1, C and D). The expression of iNS1 after infection of HuH-7 cells with wild-type or T164S virus was also similar as shown by Western blotting (Fig. 2F) and quantification of NS1 by enzyme-linked immunosorbent assay (ELISA) (Fig. 2G).

An increase in secreted sNS1 was observed for T164S virus compared to wild-type virus irrespective of the starting MOI (MOI 1: twofold, $P = 0.029$; MOI 10: fourfold, $P = 0.037$) (Fig. 2H). This suggested greater secretion efficiency for mutant NS1 compared to wild-type NS1. There was no readily observable difference in plaque size or morphology for T164S virus compared to wild-type virus (fig. S1E). Furthermore, the T164S mutation was found to be stably maintained through 10 alternate passages between C6/36 cells and HuH-7 cells without any additional genetic changes, as revealed by viral genome sequencing. Together, our data suggest that the T164S mutation in sNS1 may have an impact on early infectious virus production and NS1 secretion without affecting viral RNA replication.

T164S mutant virus is better able to infect mosquitoes than wild-type virus

Next, we examined the impact of the T164S mutation of NS1 on mosquito infectivity (14–16). First, we orally infected the mosquito vector of dengue, *Aedes aegypti*, with either T164S mutant or wild-type virus at three different inocula (10^5 to 10^7 pfu/ml of specific pathogen-free pig blood) and then examined the viral load on day 9 after infection (fig. S2A). The viral load in the mosquitoes was determined by RT-PCR at each infection inoculum, and no difference in the percentage of infected mosquitoes was found (fig. S2B). A nearly twofold higher viral load was observed for T164S mutant virus-infected mosquitoes at the lower infection doses (fig. S2B), which correlated with higher amounts of sNS1 in the blood meal (fig. S2C). This suggested that the T164S mutant virus may have a replication advantage. Next, *A. aegypti* mosquitoes were orally infected with T164S mutant virus or wild-type virus (5×10^5 pfu/ml) in a pig blood meal, and the viral replication kinetics in mosquito midguts on days 1 and 3 after infection were examined. Viral replication by day 3 after infection was 4.8-fold higher in T164S mutant virus-infected mosquitoes compared to wild-type virus-infected mosquitoes (Fig. 3A). The viral load in the midguts of T164S mutant virus-infected mosquitoes was 1.9-fold higher than in wild-type virus-infected mosquitoes on day 1 after infection and was significantly higher (4.8-fold) on day 3 after infection ($P = 0.026$) (Fig. 3B). The number of T164S mutant virus-infected mosquito midguts (>10 pfu) was higher (11 of 30 midguts, 36.7%) than for wild-type virus-infected mosquito midguts (6 of 30 midguts, 20%) (Fig. 3C). Examination of viral load in salivary glands and whole mosquito carcasses on day 7 after infection showed that T164S mutant virus was capable of dissemination within the mosquito, with a 1.4-fold higher viral load for T164S mutant virus compared to wild-type virus (Fig. 3D). More NS1 was expressed in the midguts of T164S virus-infected mosquitoes than in the midguts of wild-type virus-infected mosquitoes, as demonstrated by Western blotting (Fig. 3, E and F), NS1-capture ELISA (Fig. 3G), and immunofluorescence assay (fig. S2D). Furthermore, higher expression of T164S mutant NS1 was detected in the mosquito salivary glands by Western blotting analysis (fig. S2E) and NS1-capture ELISA (fig. S2F) on day 7 after infection compared to wild-type NS1. A potential replication advantage for T164S mutant virus was further supported by higher expression of virus-encoded NS3 (Fig. 3E) and an increase in viral GCs (Fig. 3A).

Increased sNS1 production after ex vivo infection of human PBMCs by T164S mutant virus compared to wild-type virus

We examined the ability of T164S mutant virus and wild-type virus at an MOI of 10 to infect human PBMCs from three independent

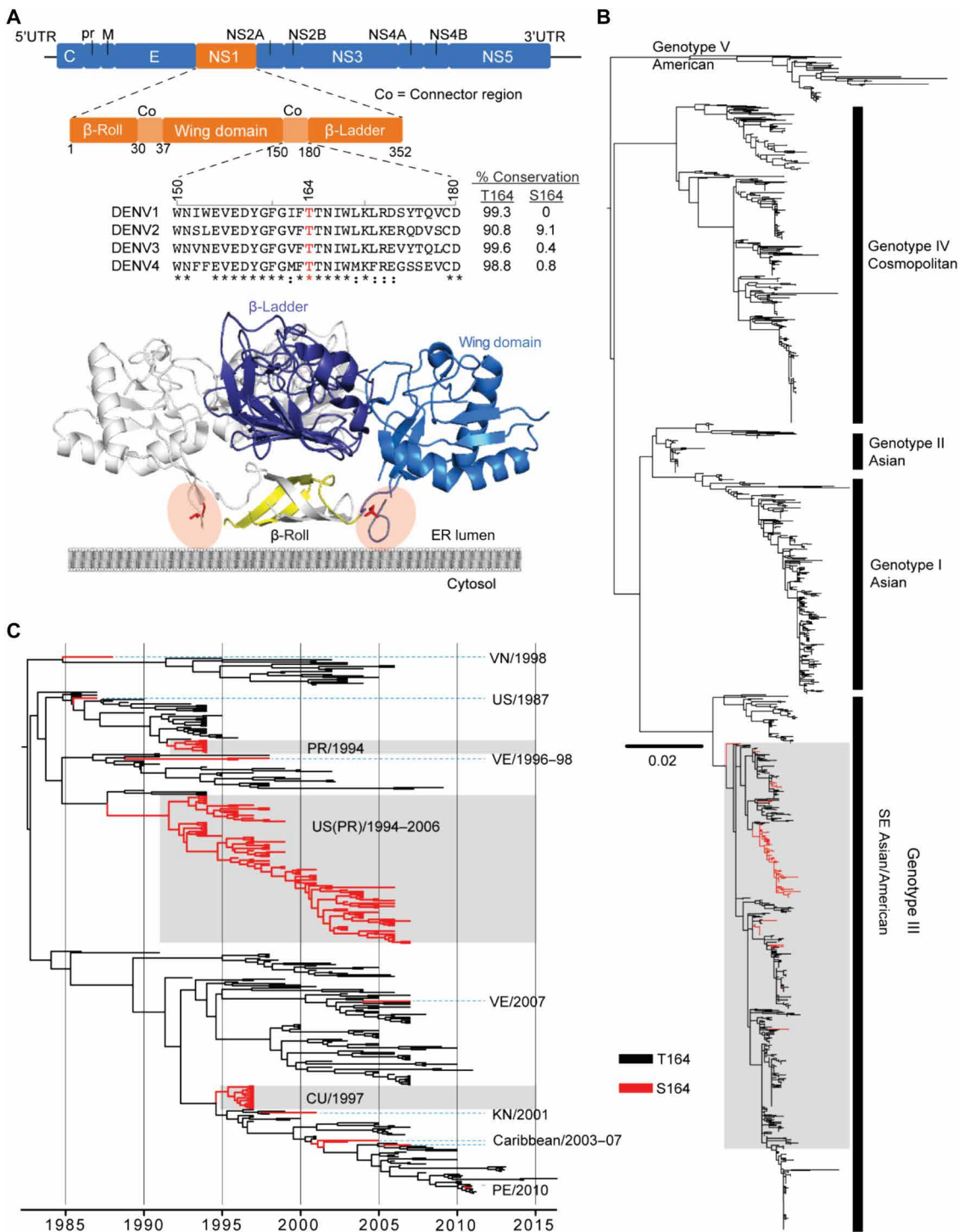


Fig. 1. Conservation, spatial location, and phylogenetic distribution of dengue virus NS1 residue 164. (A) Organization of the dengue virus genome indicating structural (C, capsid; prM, premembrane; E, envelope) and nonstructural (NS1 to NS5) genes flanked by 5' and 3'UTRs (untranslated regions). Sequence alignment of the connector (Co) subdomain (residues 150 to 180) is shown for DENV1 to DENV4 (represented by selected strains with the following GenBank accession numbers: EU081230.1, EU081177.1, EU081190.1, and GQ398256.1, respectively). The percent (%) conservation of residues T164 and S164 across dengue virus serotypes was estimated using the total number (*n*) of publicly available NS1 sequences for DENV1 (*n* = 1868), DENV2 (*n* = 1590), DENV3 (*n* = 1020), and DENV4 (*n* = 243) in the Virus Pathogen Database and Analysis Resource [ViPR database (10) as of 28 March 2017]. The 3D structure of the dengue virus NS1 dimer [Protein Data Bank (PDB) 4O6B] (11) showing one monomer in color (β -roll, yellow; β -ladder, purple; wing domain, blue) and the other monomer in gray is depicted. The greasy finger loop (residues 159 to 162, shaded in pink for both monomers) is based on the West Nile virus NS1 dimer (PDB 4O6D), with residue T164 indicated (red stick) for both monomers. ER, endoplasmic reticulum. (B) Evolutionary relationship of DENV2 strains showing that the T164S mutation is distributed exclusively within the American clade of DENV2 genotype III. (C) Bayesian molecular clock showing the spatiotemporal distribution of the T164S mutation within the Southeast (SE) Asian/American genotype III clade.

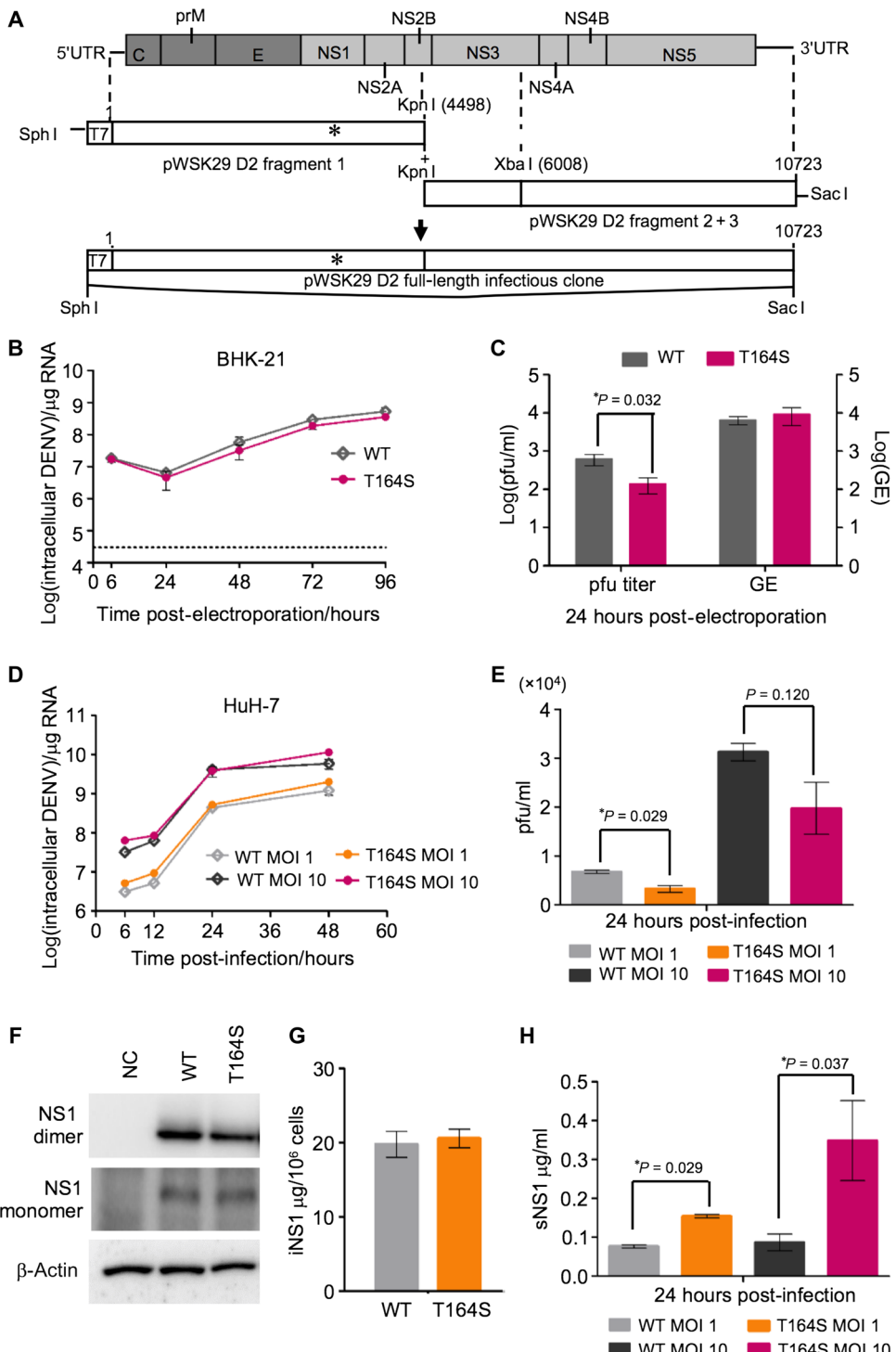


Fig. 2. Characterization of the T164S mutation in NS1 of dengue virus. (A) Dengue virus serotype 2 3295 strain infectious clone (GenBank accession number EU081177.1) indicating standard genetic manipulations for introduction of the T164S mutation into NS1 (asterisks). (B) Real-time PCR quantification of intracellular viral RNA at the indicated time points after electroporation of BHK-21 cells with wild-type or T164S mutant virus. The dashed line represents the detection level for the mock-transfected control BHK-21 cells. WT, wild type. (C) Virus titer in infected BHK-21 cell supernatants at 24 hours after transfection with either wild-type or T164S mutant virus, which was determined using a plaque assay (left axis). The GE shown on the right axis is the ratio of extracellular RNA GCs measured by RT-PCR to infectious virus measured by plaque assay (pfu). (D) Real-time PCR quantification of wild-type or T164S mutant virus genome replication at an MOI of 1 or 10 in infected HuH-7 liver cells. (E) Supernatants from infected HuH-7 cells 24 hours after infection were subjected to plaque quantification (pfu/ml). (F) Nonreducing SDS-polyacrylamide gel electrophoresis (SDS-PAGE) of the cell lysates from (D). (G) Intracellular NS1 (iNS1) quantification in cell lysates from (D) measured by ELISA. (H) Quantification of sNS1 in the supernatants from cells in (D) measured by ELISA. Data are presented as means \pm SD from duplicate of two independent experiments, and differences between wild-type and T164S mutant virus groups were compared by Mann-Whitney test (*P < 0.05).

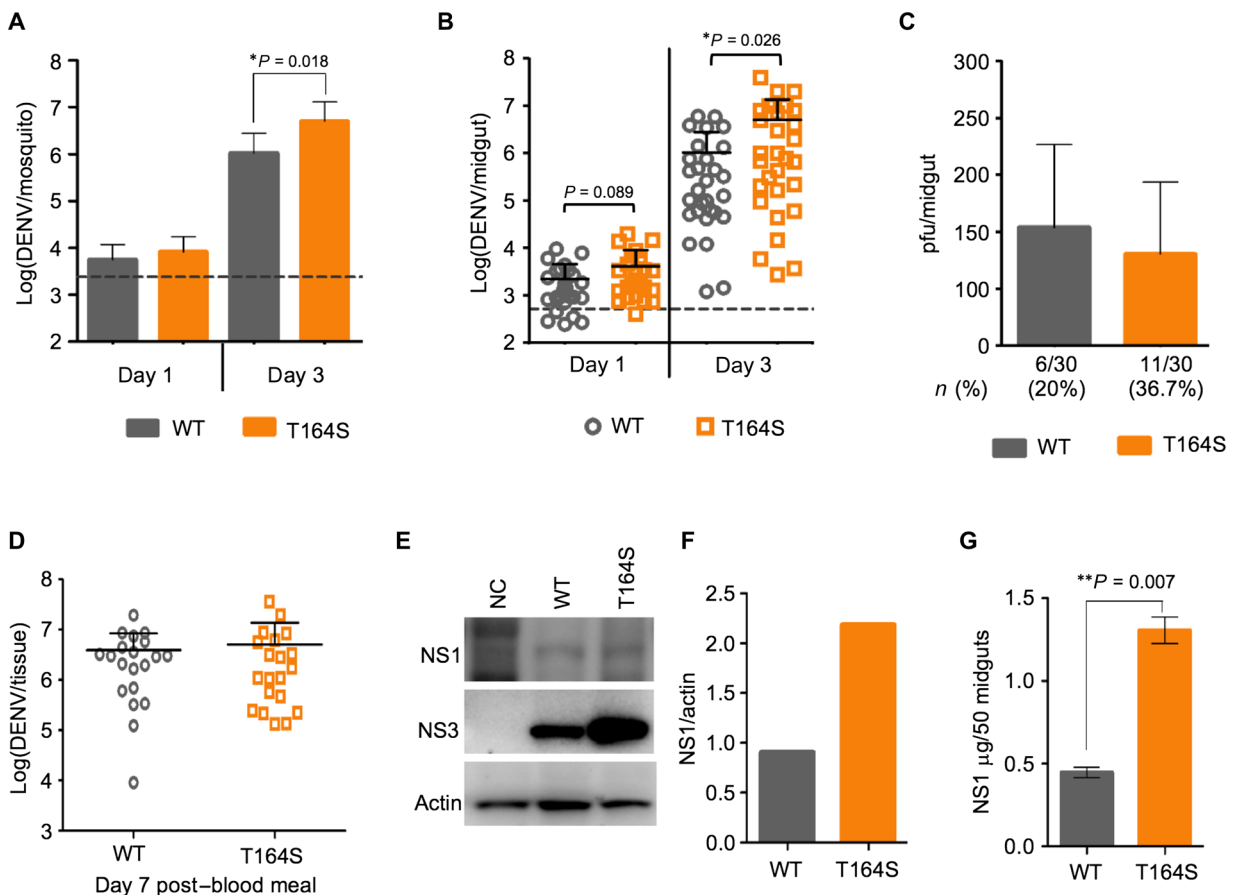


Fig. 3. Replication kinetics of wild-type or T164S mutant dengue virus in the *A. aegypti* mosquito vector. *A. aegypti* mosquitoes were infected with wild-type or T164S mutant virus (5×10^5 pfu/ml) through a blood meal, and midgut viral loads were compared to those of whole carcasses. (A) Average viral load in whole mosquito carcasses obtained by summing the midgut and carcass viral loads ($n = 30$). (B) Scatter plot showing the viral load of individual mosquito midguts from (A) quantified by real-time PCR. (C) Average infectious viral titer of mosquito midgut homogenates at day 3 after infection based on the number of midgut homogenates with a virus titer > 10 pfu. (D) Scatter plot of the viral loads in individual mosquito salivary glands and carcasses [from (A)] on day 7 after infection measured by real-time PCR. (E) Western blot of NS1 and NS3 proteins in homogenates from 50 mosquito midguts. (F) The band intensity of NS1 from (E) was normalized to that of β -actin using ImageJ. (G) The total NS1 in the mosquito gut homogenates was quantitated by ELISA. Mean values for wild-type and mutant NS1 were compared by Mann-Whitney test. Mean values of mosquito gut viral loads between the wild-type and T164S mutant virus groups were compared by the Mann-Whitney test. Data are presented as means \pm SD from three independent experiments, and significance is indicated as *P < 0.05.

donors in the absence or presence of a humanized 4G2 antibody. This antibody is against the viral envelope protein and facilitates antibody-dependent enhancement (ADE) of viral infectivity (17). Similar to infection of BHK-21 cells and HuH-7 cells, the production of T164S mutant virus in human PBMCs was suppressed 24 hours after infection compared to wild-type virus (Fig. 4A). Quantification of viral GCs in the supernatants from infected human PBMCs and measurement of the GE revealed no differences between T164S mutant virus– and wild-type virus–infected cells (fig. S3, A and B). Quantification of sNS1 in the cell supernatants by capture ELISA revealed greater sNS1 production by T164S mutant virus–infected cells compared to wild-type virus–infected cells (Fig. 4B). Next, we measured the proinflammatory cytokines interleukin-6 (IL-6) and tumor necrosis factor α (TNF α) in the PBMC supernatants by ELISA (18). IL-6 production was 3.7-fold higher for the T164S mutant virus–infected cells compared to wild-type virus–infected cells in the presence of 4G2 antibody Fig. 4C). TNF α was increased by 2.7-fold for T164S virus–infected compared to wild-type virus–infected cells in the presence of 4G2 antibody (Fig. 4D). Moreover, in the PBMC infection

assay in the absence of 4G2 antibody, IL-6 and TNF α production could be measured for the T164S mutant virus but not for the wild-type virus (Fig. 4, C and D), although wild-type virus showed higher production of virions (Fig. 4A).

We then investigated whether sNS1 from the T164S mutant virus could be responsible for the proinflammatory response observed in the human PBMCs ex vivo. We purified sNS1 from supernatants of BHK-21 cells infected with T164S mutant virus or wild-type virus using immunoaffinity chromatography (~50 to 80% purity; fig. S3C) (19) and found that sNS1 from both mutant and wild-type viruses was in the form of stable hexamers (Fig. 4E). Incubation of human PBMCs with purified sNS1 from T164S mutant virus resulted in about twofold greater production of IL-6 (Fig. 4F) and TNF α (Fig. 4G) compared to sNS1 from wild-type virus irrespective of the amount of sNS1 used.

We then probed expression of 268 inflammatory genes in the virus-infected human PBMCs using the NanoString gene counting platform (20). Our probe pool contained probes not only for host inflammatory genes but also for the 5' and 3' ends of the DENV genome as internal

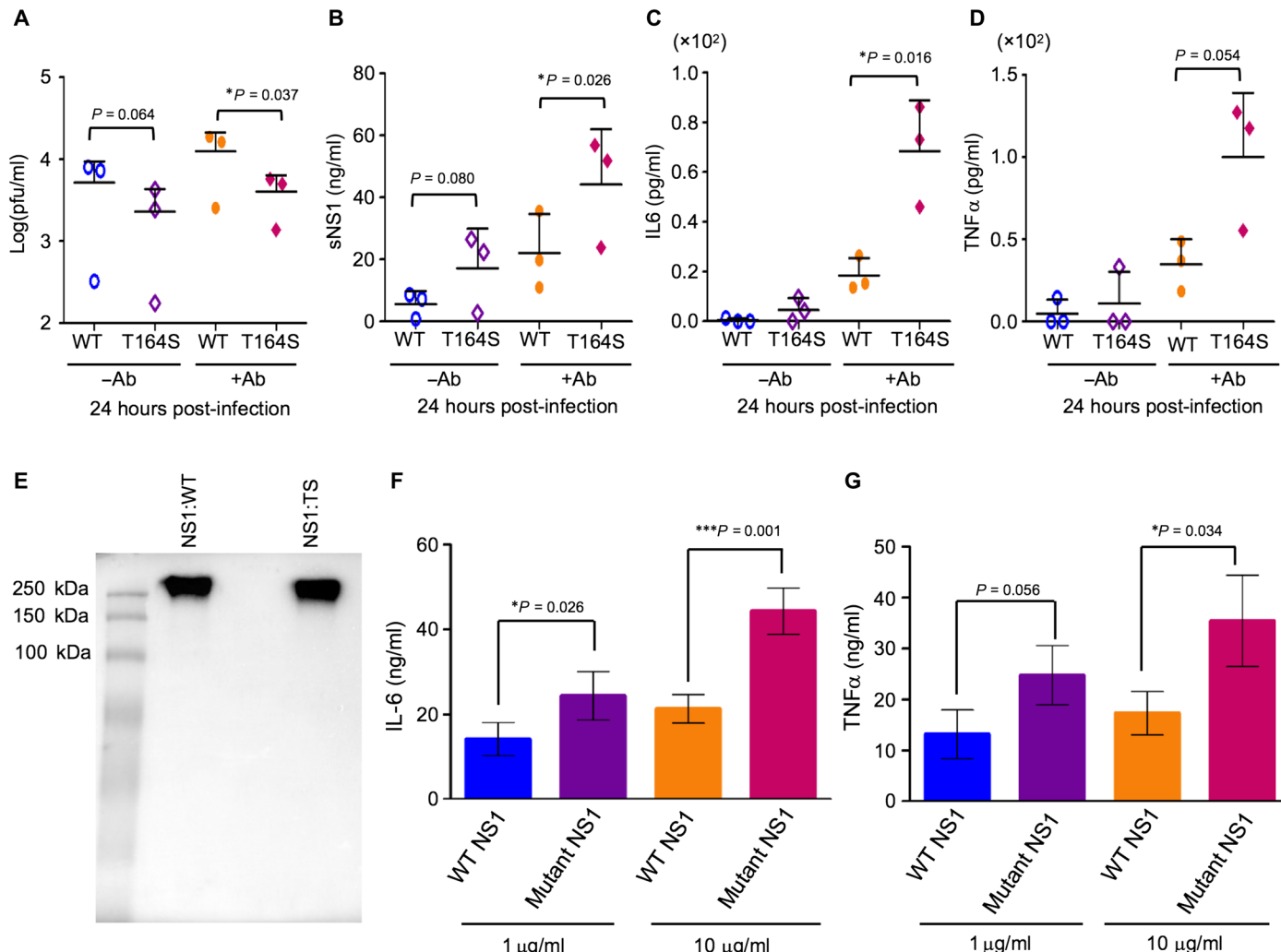


Fig. 4. Infection of human PBMCs ex vivo with wild-type or T164S mutant dengue virus in the absence or presence of humanized 4G2 antibody. Human PBMCs ($n=3$ donors) were infected with 10^7 pfu (MOI = 10) of wild-type or T164S mutant virus either alone or in an immune complex with 0.05 μ g of the humanized 4G2 antibody (Ab) (17). Supernatants were collected at 24 hours after infection and were analyzed as follows: (A) infectious virus titer quantification by plaque assay, (B) sNS1 measurement by ELISA, and (C) IL-6 and (D) TNF α concentrations measured by ELISA. (E) Native SDS-PAGE Western blot of wild-type and T164S mutant virus sNS1 purified from BHK-21 cell supernatants. (F) IL-6 and (G) TNF α concentrations were measured in the supernatants of human PBMCs incubated with purified wild-type or T164S mutant sNS1 (either 1 or 10 μ g/ml) for 24 hours. Data are presented as scatter plots or bar graphs and show means \pm SD from three independent experiments. Differences between the wild-type virus and T164S mutant virus were compared by Mann-Whitney test (* $P < 0.05$).

controls for detecting virus infection. We assessed infectivity and subgenomic flaviviral RNA (sfRNA) in T164S mutant virus- and wild-type virus-infected human PBMCs because previous studies have shown that these characteristics can affect host inflammatory gene expression (21). We found consistently higher expression of the 3'UTR compared to the virus envelope gene with a ratio of 2:1, which we attributed to sfRNA transcripts (fig. S3D). The sfRNA to viral genomic RNA ratio showed no difference between T164S mutant virus and wild-type virus (fig. S3D). Transcription of IL-6 and TNF α genes was slightly higher at 6 hours after infection for T164S mutant virus-infected human PBMCs compared to wild-type virus-infected human PBMCs (fig. S3, E and F, respectively).

Of the 268 inflammatory genes profiled, 35.8% (96 of 268 genes) and 45.1% (121 of 268 genes) were expressed at a higher level during the course of human PBMC infection with wild-type or T164S mutant virus in the absence or presence of humanized 4G2 antibody

compared to uninfected PBMCs (calculated as \log_2 fold changes; figs. S4 and S5). The most highly up-regulated genes were the type 1 IFN response genes (IFN α/β , IFITs, OAS, MX1, and MX2) and the genes encoding cytokines IL-1 and IL-8. These have been previously reported to be up-regulated in dengue virus-infected human liver HepG2 cells and in patients with dengue virus infection (22, 23). Further examination of the overall regulation of the inflammation-associated genes in T164S mutant virus-infected human PBMCs revealed that most of the genes encoding cytokines, nuclear factor κ B (NF κ B), complement, Janus kinase (Jak)-signal transducer and activator of transcription (STAT), mitogen-activated protein kinase (MAPK), TLR-related proteins, and protein targeting to glycogen (PTG) were up-regulated at 6 hours after infection (fig. S6). These genes were more prominently up-regulated at 6 hours after infection with T164S mutant virus compared to wild-type virus in the presence of humanized 4G2 antibody (fig. S7).

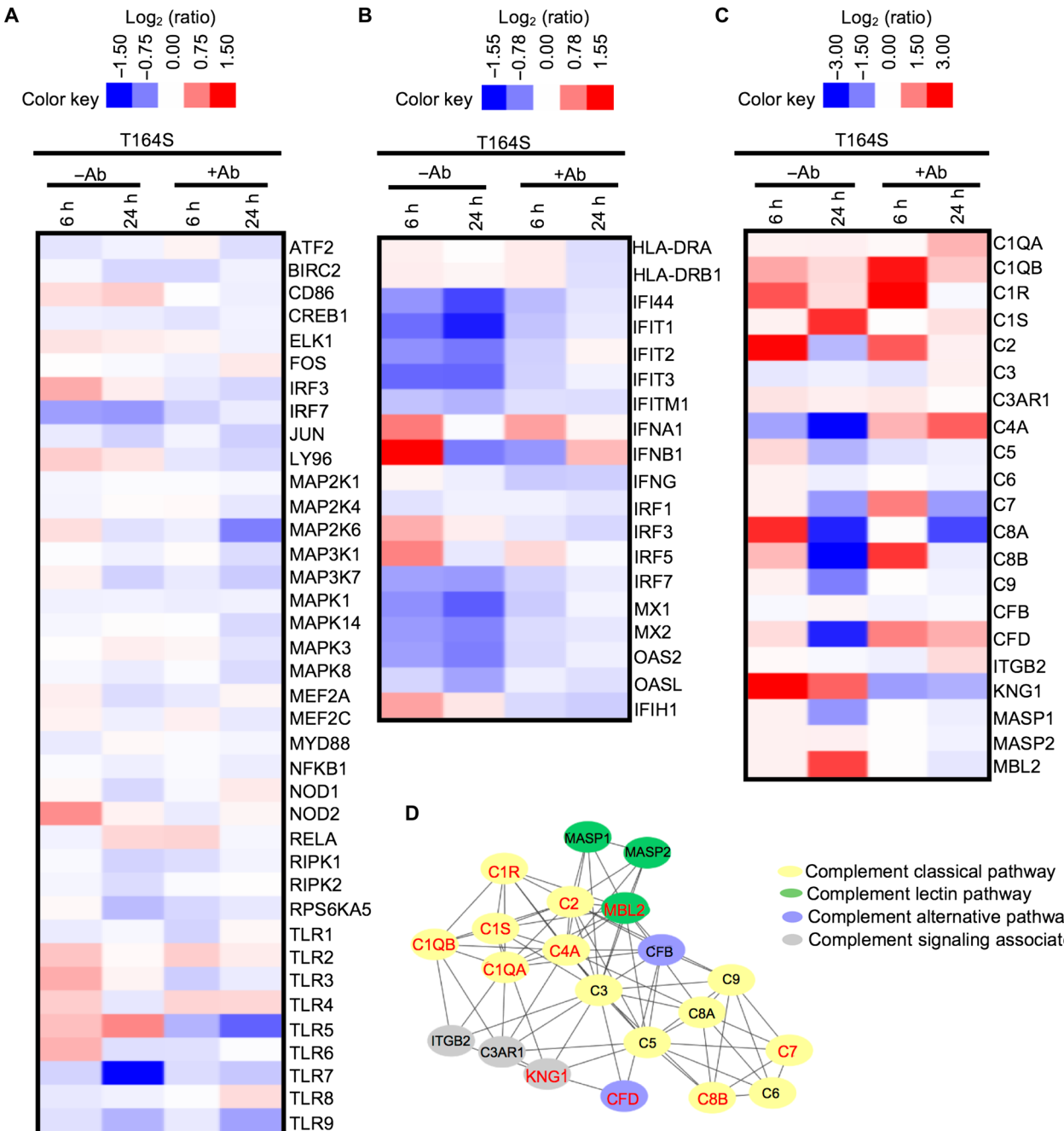


Fig. 5. Expression of inflammation-associated genes after infection of human PBMCs with wild-type or T164S mutant dengue virus. Human PBMCs ($n=2$ donors) were infected with 10^7 pfu (MOI = 10) of wild-type or T164S mutant virus either alone or in an immune complex with 0.05 μg of the humanized 4G2 antibody (17). Total RNA was extracted from human PBMCs at 6 and 24 hours after infection, and gene expression analysis was performed using custom probes (table S1). Gene expression was normalized to that of the panel's internal housekeeping genes. Normalized gene expression of the T164S mutant virus was then expressed as \log_2 fold change with respect to wild-type virus. Clusters of gene expression in the heat maps are based on KEGG (Kyoto Encyclopedia of Genes and Genomes)/Gene Ontology analysis. (A) Heat map of expression of MyD88-dependent/TLR signaling pathway genes. (B) Heat map of expression of cytokine/IFN-mediated signaling pathway genes. (C) Heat map of expression of complement cascade genes. (D) STRING analysis showing interaction network of the complement cascade genes in the gene expression panel generated by Cytoscape (43). Genes in red are those that are highly up-regulated (\log_2 fold change ≥ 1.5) in human PBMCs after infection by the T164S mutant virus. Data presented are from two independent experiments.

Infection of human PBMCs with T164S mutant virus also resulted in up-regulation of genes associated with MyD88-dependent TLR signaling (Fig. 5A), cytokine/IFN-mediated signaling (Fig. 5B), and complement signaling (Fig. 5C) at 6 hours after infection. Consistent

with previous reports, TLR2 (24) and TLR4 (7, 8), which are associated with vascular leakage and the severity of dengue disease, were highly expressed during T164S mutant virus infection of human PBMCs in the presence or absence of humanized 4G2 antibody (Fig. 5A).

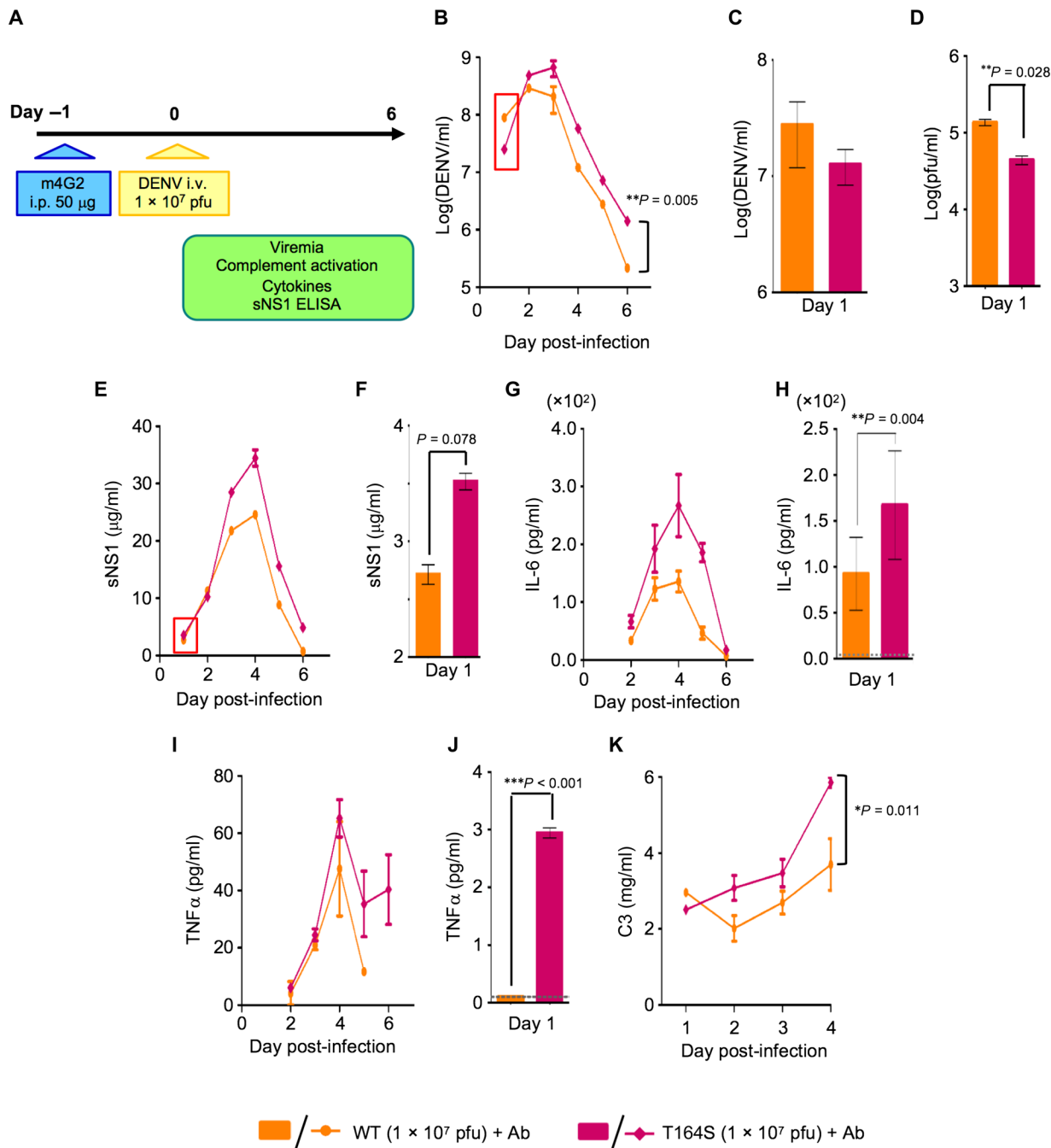


Fig. 6. Nonlethal infection of AG129 mice with wild-type or T164S mutant virus. (A) Schematic showing the timeline of nonlethal infection of AG129 mice with wild-type or T164S mutant virus and daily sampling for analysis of virus replication and proinflammatory markers. AG129 mice ($n=6$ per group) were given 50 µg of mouse 4G2 antibody intraperitoneally 1 day before intravenous injection of 10^7 pfu ($\sim 5 \times 10^{11}$ GE) of wild-type or T164S mutant virus. (B) Viremia kinetics were measured by PCR in pooled serum collected from mice infected with wild-type virus or T164S mutant virus. (C) Average viremia on day 1 after infection of mice infected with wild-type or T164S mutant virus. (D) The average infectious titer on day 1 after infection was measured in mouse serum by a plaque assay. (E) The amount of sNS1 in mouse serum was measured by ELISA. (F) Average amount of sNS1 produced on day 1 after infection. (G to K) Mouse serum concentrations of proinflammatory cytokines measured by ELISA for (G and H) IL-6, (I and J) TNF α , and (K) complement C3. Mouse serum concentrations for day 1 after infection for (H) IL-6 and (J) TNF α . Differences in viremia kinetics and serum complement C3 concentrations between wild-type virus– and T164S mutant virus–infected mouse groups were compared by two-way analysis of variance (ANOVA) with Bonferroni correction. Data are presented as means \pm SD from two independent experiments, and differences between wild-type virus– and T164S mutant virus–infected mouse groups were compared by Mann-Whitney test (*P < 0.05 and **P < 0.01). i.p., intraperitoneally; i.v., intravenously.

However, TLR6 (24) was only up-regulated during T164S mutant virus infection in the absence of humanized 4G2 antibody (Fig. 5A). Expression of downstream IFN-stimulated genes in T164S mutant

virus–infected PBMCs was reduced compared to wild-type virus–infected PBMCs, although the former cells showed greater transcription of genes encoding type 1 IFN α/β (Fig. 5B).

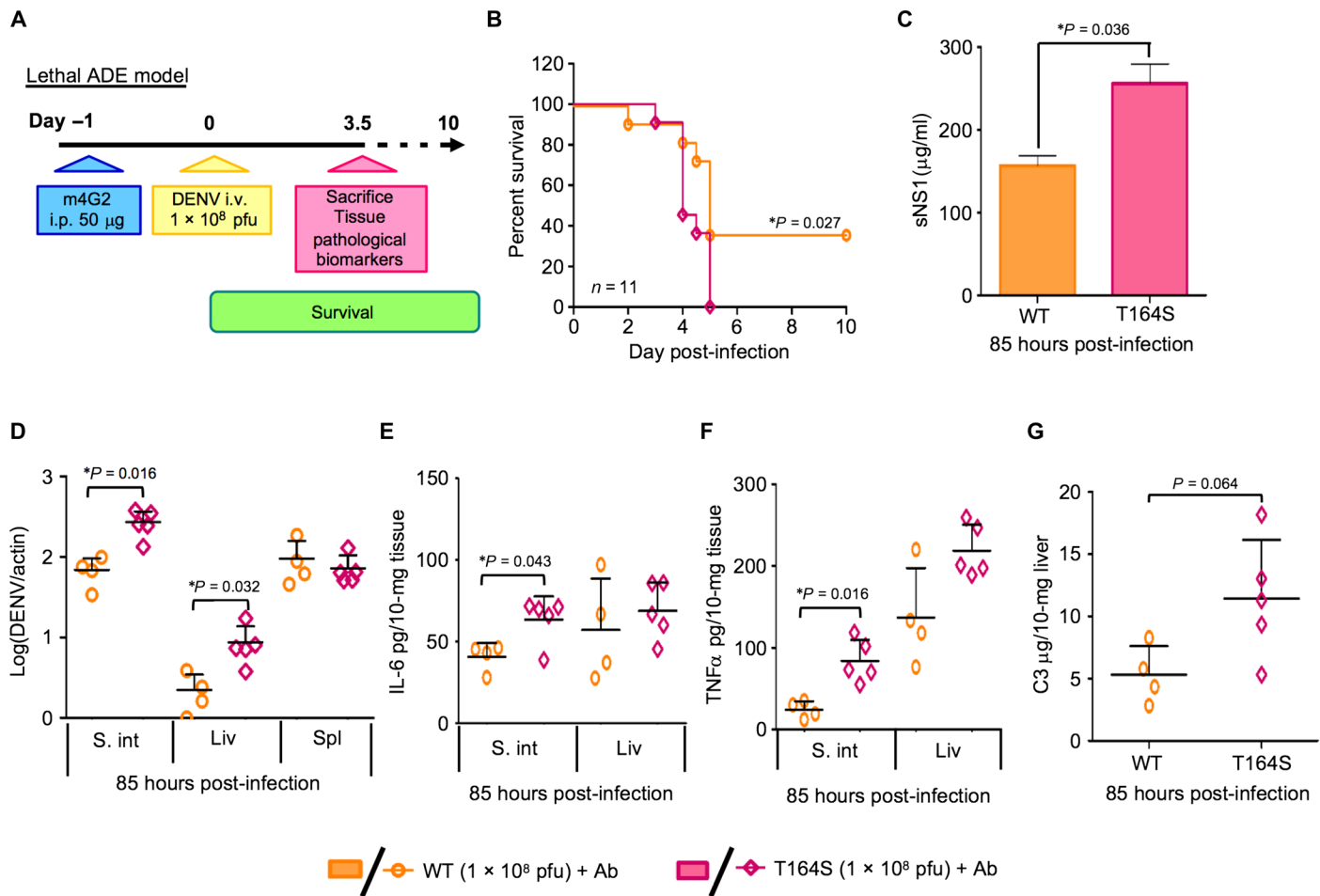


Fig. 7. Lethal infection of AG129 mice with wild-type or T164S mutant dengue virus. (A) The schematic shows the timeline of the experiment. AG129 mice were given 50 µg of 4G2 mouse antibody intraperitoneally and were injected intravenously 1 day later with 10⁸ pfu (~5 × 10¹² GE) of wild-type or T164S mutant virus (*n* = 5 or 6 per group). Mouse survival was monitored for 10 days after infection (27). In addition, two to three mice were independently infected and sacrificed at ~85 hours after infection, and their tissue viral load and pathological markers were measured. (B) Survival plots (log-rank Mantel-Cox test) for AG129 mice infected with wild-type or T164S mutant virus. (C) Mouse serum sNS1 was measured at 85 hours after infection by ELISA. (D) Viral load in mouse tissues [small intestine (S. int), liver (Liv), and spleen (Spl)] was measured by PCR, and the viral RNA expression was normalized to actin expression. (E to G) Concentrations of (E) IL-6, (F) TNF α , and (G) complement C3 were measured in mouse tissue homogenates by ELISA. Data points shown as scatter plots (D to G) are means \pm SD from two independent experiments. Differences between wild-type virus and T164S mutant virus were compared by Mann-Whitney test (*P < 0.05).

Given that the association of viral NS1 with vascular leakage in dengue disease (6–8) also involves complement-associated genes, we subjected these genes to STRING and KEGG pathway analysis. Our data showed an interactome of genes up-regulated in T164S mutant virus-infected PBMCs (Fig. 5D). Most of the complement-associated genes were up-regulated about twofold throughout the course of T164S mutant virus infection (Fig. 5D). The interacting network of genes was found to belong to the classical complement activation pathway (Fig. 5, C and D) that has been linked to severe dengue disease (25). Furthermore, MBL2 (in the complement lectin pathway) and KNG1 (associated with complement signaling) were up-regulated greater than threefold in T164S mutant virus-infected cells only in the absence of antibody (Fig. 5C).

T164S mutant virus induces more severe disease in AG129 mice compared to wild-type virus

Next, we probed the biological relevance of our findings in the ex vivo human PBMC infection system in a nonlethal mouse model of dengue

virus infection (26). We infected AG129 mice with T164S virus or wild-type virus in the presence or absence of mouse 4G2 antibody and examined viremia, complement activation, and production of sNS1 and cytokines at various time points after infection (Fig. 6A). The overall kinetics of production of virus measured by RT-PCR and plaque assay, sNS1, and inflammation-related proteins in mice infected with T164S mutant virus or wild-type virus was similar to previous studies (Fig. 6) (26, 27). Early events at day 1 after infection showed a similar trend to those in our ex vivo PBMC infection system (Figs. 2 and 4). T164S mutant virus-infected mice showed reduced viral RNA production (P = 0.010) (Fig. 6, B and C) and infectious virus production (P = 0.028) compared to mice infected with wild-type virus on day 1 after infection despite the use of an identical starting inoculum for both viruses (Fig. 6D). Serum sNS1 was higher for T164S mutant virus-infected mice compared to wild-type virus-infected mice (Fig. 6, E and F). IL-6 and TNF α concentrations (28, 29) in pooled serum (*n* = 6) were also significantly higher for T164S mutant virus-infected mice at day 1 after infection compared to

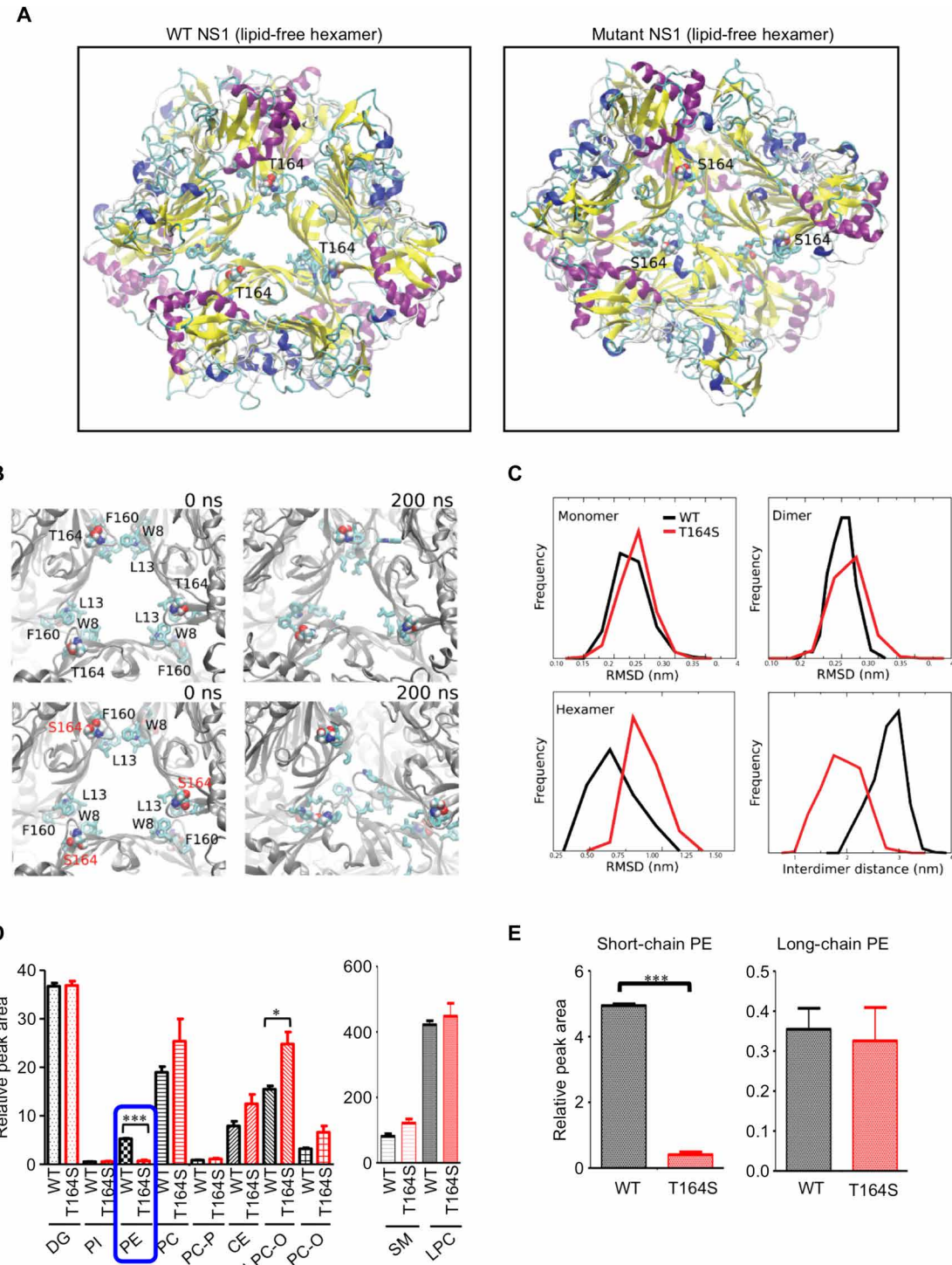


Fig. 8. Molecular simulations and lipid analysis of wild-type and mutant hexameric NS1. (A) Snapshot simulations of wild-type NS1 (left) and T164S mutant NS1 (right) in a lipid-free system with amino acid residue T164 labeled. (B) Zoomed-in initial (0 ns, left) and final (200 ns, right) snapshots of the wild-type (top) and T164S mutant (bottom) NS1 hexamer highlighting the hydrophobic interface between adjacent NS1 dimers (shown in wireframe format with labeling of the amino acids at the dimer interface involved in hydrophobic interactions). (C) Distribution of protein backbone root mean square deviations (RMSD) with respect to the x-ray structure as well as the minimum distance between interdimer hydrophobic clusters for wild-type (black) and T164S mutant (red) NS1. The NS1 monomer (top left), NS1 dimer (top right), and NS1 hexamer (bottom left) are shown. The bottom right panel shows the interdimer distance of wild-type (black) and T164S mutant (red) NS1. (D) Relative abundance of major lipid classes extracted from immunoaffinity-purified wild-type or T164S mutant sNS1 determined by LC-MS/MS. DG, diacylglycerols; PI, phosphatidylinositol; PE, phosphatidylethanolamines; PC, phosphatidylcholines; CE, cholesterol esters; LPC-O, ether lysophosphatidylcholines; PC-O, ether phosphatidylcholines; SM, sphingomyelins. (E) Relative abundance of short-chain phosphatidylethanolamine (PE) subclasses (carbon length of 32 to 34 atoms) for immunoaffinity-purified wild-type and T164S mutant sNS1 [blue box in (D)]. Data are presented as means \pm SD from three independent experiments and were compared by unpaired two-tailed Student *t* test (**P* < 0.05 and ****P* < 0.001).

wild-type virus-infected mice ($P = 0.007$: Fig. 6, G and H, and $P = 0.004$: Fig. 6, I and J, respectively). The decreased viral load in serum and enhanced production of the proinflammatory cytokine IL-6 on day 1 after infection in T164S mutant virus-infected mice was also found during infection in the absence of 4G2 antibody [3.0-fold lower viral RNA: $P < 0.001$, fig. S8 (A and B); 2.1-fold increased IL-6: $P = 0.003$, fig. S8 (C and D)]. We next measured complement C3 in pooled serum ($n = 6$) and found a significant increase over the course of infection in T164S mutant virus-infected mice compared to mice infected with wild-type virus (in the absence of mouse 4G2 antibody: $P = 0.044$, fig. S8E; in the presence of mouse 4G2 antibody: $P = 0.011$, Fig. 6K).

We next used the AG129 lethal infection mouse model (27) to investigate whether T164S mutant virus infection caused more severe disease in these animals compared to wild-type virus (Fig. 7A). Mice infected with the T164S mutant virus showed earlier mortality (median survival of 4 days; 100% lethality) compared to mice infected with wild-type virus (median survival of 5 days; 60% lethality; $P = 0.027$) (Fig. 7B). Data for one mouse from the wild-type virus-infected group were excluded from subsequent analysis because of its unusual early death on day 2 after infection (27). The increased mortality of the mice infected with T164S mutant virus corresponded to an overall higher viremia with a 2.1-fold ($P = 0.073$) and 4.5-fold ($P = 0.004$) higher serum viral load compared to mice infected with wild-type virus on days 3 and 4 after infection, respectively (fig. S8F). These higher viral loads were coupled with a slight increase in the amount of systemic sNS1 measured on day 3.5 after infection ($P = 0.036$; Fig. 7C). We examined the viral load and proinflammatory protein production in the small intestine, liver, and spleen on day 3.5 after infection because these are the major organ sites of severe pathology associated with ADE of dengue virus infection (27–29). Mice infected with the T164S mutant virus displayed a higher viral load than did mice infected with wild-type virus in the small intestine (3.9-fold, $P = 0.016$) and liver (4.0-fold, $P = 0.032$), but no difference in viral load was noted in the spleen (Fig. 7D). The higher viral load correlated with higher IL-6 and TNF α concentrations in serum (fig. S8, G and H) and tissues (small intestine, Fig. 7E; liver, Fig. 7F) in the T164S mutant virus-infected mice compared to wild-type virus-infected mice. Complement C3 in the liver where it is predominantly synthesized (30) was 2.2-fold higher ($P = 0.064$) in T164S mutant virus-infected mice compared to wild-type virus-infected mice (Fig. 7G).

The T164S mutation is predicted to make hexameric NS1 unstable

We next performed atomic-resolution molecular dynamics simulations of the T164S and wild-type hexameric NS1 protein using the GROMACS 5.1.4 molecular dynamics simulation package. Three replica simulations of 200 ns each were performed per system to improve the sampling of the conformational space of the wild-type and T164S mutant NS1 proteins. The wild-type hexameric complex exhibited a relatively stable structure that was comparable to the x-ray structure (PDB ID, 4O6B) (11), with an approximate threefold symmetry around the three dimers and a central pore known to contain a lipid cargo (Fig. 8A, left) (5, 11). In contrast, simulation of the T164S mutant NS1 hexameric complex led to a pronounced collapse of the symmetrical arrangement, thus occluding the central lipid-containing pore (Fig. 8A, right). In the wild-type protein, the methyl group at the side chain of T164 contributes to a hydrophobic interaction cluster that includes amino acid residues W8, L13, and F160, which

stabilize the interface between symmetrical pairs of dimers (Fig. 8B, top). The loss of a total of six methyl groups in the T164S mutant hexameric complex causes a reduction in packing at each interface that is needed to maintain the symmetrical hydrophobic interaction network between the mutant NS1 dimers (Fig. 8B, bottom). The root mean square deviation of the protein backbone of the wild-type and T164S mutant NS1 was quantified to provide measurements of the structural drift of the hexameric NS1 and its individual components, relative to the x-ray structure. Whereas monomers and dimers within both the wild-type and mutant NS1 hexamers exhibited limited structural drift (~0.25 nm) (Fig. 8C, top), the entire hexamer showed greater tendency to drift from the x-ray structure in the T164S mutant NS1 compared to wild-type NS1 (Fig. 8C, bottom left). The distribution of distances between hydrophobic clusters of the dimers was measured for both wild-type and T164S mutant hexameric NS1 (Fig. 8C, bottom right). This confirmed that whereas the wild-type NS1 stably maintained a mean separation at each dimer interface of ~3 nm, the loss of packing within the T164S mutant NS1 led to an oscillation of about half this distance (Fig. 8C, bottom right). We purified the T164S mutant NS1 hexameric complex from T164S mutant virus-infected mammalian cell culture supernatants (Fig. 4E). Lipid profiling of immunoaffinity-purified wild-type and T164S mutant NS1 hexameric complexes by liquid chromatography-tandem mass spectrometry (LC-MS/MS) identified 180 lipid molecular species (table S3). Lipid classes such as sphingomyelins and ether phosphatidylcholines were overrepresented in the T164S mutant NS1 compared to wild-type NS1, whereas phosphatidylethanolamines were reduced in the T164S mutant NS1 (Fig. 8E).

DISCUSSION

Mutations arising in dengue virus during dengue epidemics have been correlated with an increased disease severity (21), implicating viral factors in severe dengue disease (2, 31, 32). Recently, mutations in the viral 3'UTR were shown to result in the increased accumulation of sfRNA compared to genomic length RNA, which conferred epidemiological fitness to the virus by suppressing the host type 1 IFN response. These mutations were associated with the dengue virus clade that caused more severe disease in the 1994 Puerto Rico epidemic (21). A conserved amino acid substitution from threonine to serine at position 164 (T164S) in the NS1 protein of dengue virus was proposed to be associated with disease severity of the 1997 Cuban epidemic (2, 3) and subsequently was detected in several DENV2 epidemics in the Americas. Given that the contribution of the T164S substitution in NS1 to disease severity is not well understood (3), we reverse engineered this mutation into a DENV2 infectious complementary DNA (cDNA) clone derived from a mildly infectious Singapore wild-type strain (12, 13). We found that the T164S mutant virus decreased infectious virus production despite little change in intracellular viral genome replication in BHK-21 and HuH-7 cell lines and in human PBMCs. We also found that the T164S mutant virus displayed greater infectivity in mosquitoes after an oral blood meal and increased viral replication and NS1 expression in the mosquito midgut, in part, because of greater mutant sNS1 in the blood meal. This is consistent with a recent study showing that sNS1 in the serum of infected hosts facilitated efficient infection of mosquitoes (33). The T164S mutant virus infection of human PBMCs resulted in greater production of sNS1 compared to wild-type virus infection and induced higher expression of TLR signaling- and

complement-associated genes, leading to greater production of proinflammatory cytokines such as IL-6 and TNF α . Furthermore, the T164S mutant virus triggered greater systemic inflammation in AG129 mice that was partly mediated by complement activation due to increased production of C3 in serum and liver. Recent studies have shown that NS1 antagonizes complement activation in vivo by binding to complement factors C4, C1, and C4BP (34), suggesting that NS1 is an immune evasion molecule. Our findings in AG129 mice correlate with clinical observations of higher amounts of sNS1, C3a, and C5a in the plasma of patients with severe dengue before symptoms of vascular leakage (9, 35).

The T164S mutation in NS1 of DENV2 appears along the terminal branches of the phylogenetic tree including among clades that represent large epidemics in humans, suggesting that this mutation does not persist through fixation beyond the epidemic and may not have a fitness advantage during its natural nonepidemic cycle. The fitness of wild-type virus compared to the T164S mutant virus examined by the pairwise growth competition assay (36) revealed higher fitness for the wild-type virus during coinfection of HuH-7 cells (fig. S9). The T164S mutation was identified in virus strains causing dengue epidemics in the Americas but not elsewhere; hence, mutational pressure exerted by the host or mosquito genetic background cannot be excluded. An alanine to valine mutation in Zika virus NS1 protein at position 188 resulted in greater disease transmission due to increased infectivity contributed by increased sNS1 (34).

The specific molecular events that result in the early suppression of infectious virus particle production during infection by the T164S mutant virus compared to wild-type virus remain to be elucidated. Mason (37) demonstrated that NS1 may interfere with virus morphogenesis during transit of NS1 from the ER to the trans-Golgi with a potential interaction between NS1 and the viral envelope protein. More recently, Scaturro *et al.* (38) carried out extensive structure-directed mutational studies to interrogate the role of NS1 in viral replication and identified several mutations that resulted in no change in RNA replication but showed an impact on infectious virus production in vitro. This group showed interactions between mCherry-labeled NS1 and the viral envelope protein but did not elucidate why mutations that did not alter RNA replication lowered infectious virus production. Given that sNS1 is a hexamer and the central pore lined by the three dimers is filled with lipids (5), it is possible that the T164S mutation in NS1 may lead to altered lipid load in the central core. We propose that the NS1 side chain at position 164 points toward the central core where the lipid load is contained such that altered side chains could possibly result in a disequilibrium in the lipid pool required for virion assembly when NS1 and the viral envelope protein interact during transit from the ER to the trans-Golgi (fig. S10). This competition for lipids may explain reduced infectious virus production and increased sNS1 secretion by the T164S mutant virus. Both T164 and S164 NS1 dimers are stable as revealed by molecular dynamics simulations (Fig. 8C, top), suggesting that the mutation does not compromise NS1's role in viral RNA replication. Our atomic-level molecular dynamics simulations suggested that the loss of the six methyl groups of threonine in the T164S mutant protein would reduce the packing interactions at the dimer interfaces resulting in a less stable hexameric NS1. We showed that sNS1 from T164S mutant virus formed stable hexamers in vitro, suggesting that hydrophobic collapse due to reduced packing interactions at the dimer interfaces may be prevented by rapid uptake of lipids from the lipid pool, leading to a disequilibrium that limits virion assembly. When we analyzed the lipid content of immunoaffinity-

purified sNS1 from T164S mutant virus and wild-type virus by mass spectrometry, we found that sphingomyelins and ether phosphatidylcholines were overrepresented in mutant virus, whereas phosphatidylethanolamines were underrepresented. Metabolism of ether lipids is also important for the production of infectious virions by other types of viruses (39); however, the functional consequences of the altered lipid load in mutant NS1 remain to be fully elucidated. MAPK-regulated phospholipase activity is essential for infectious virus production by dengue virus and hepatitis C virus (40). Our gene expression data showed that MAPK genes were up-regulated in the first 6 hours after infection in T164S mutant virus compared to wild-type virus.

Our study has a number of limitations. The first is the relevance of the AG129 mouse model to human dengue disease (41). A second limitation is that the transmissibility of the T164S mutant virus in the mosquito host needs to be examined using a mouse model (42) to establish the contribution of sNS1 and particularly to probe the role of its lipid content. The T164S mutant virus induced an increase in complement C3 in mice, but future studies need to test whether blocking C3 production during dengue virus infection could provide a therapeutic benefit against severe dengue disease. Last, extending the investigation of the T164S mutation to other dengue virus serotypes as well as comparing the effects of injecting mice with purified sNS1 from T164S mutant virus or wild-type virus should inform structure-activity relationships and the ability of mutant sNS1 to cause severe disease. Our findings may provide new insights into the complex interplay of viral fitness and dengue virus pathogenesis mediated by the NS1 protein.

MATERIALS AND METHODS

Study design

We aimed to investigate the mechanisms underlying the disease severity associated with the T164S mutation in the NS1 protein of dengue virus (3). We inferred the emergence and spread of this mutation through phylogenetic analysis using publicly available dengue virus sequences. The T164S mutation was reverse engineered into a DENV2 mildly infectious strain. The T164S mutant virus was analyzed in vitro in BHK-21 cells, HuH-7 cells, and human PBMCs and in vivo in the AG129 type 1 and 2 IFN receptor-deficient mouse. Virus replication was assessed by quantification of viral RNA and infectious virus production in cell lines in vitro. The magnitude of sNS1 protein secretion was measured by capture ELISA. The effect of mutant sNS1 on the ability of mutant virus to infect mosquitoes was analyzed. We assessed the contribution of the T164S mutation in NS1 to inflammation using a human PBMC infection assay to measure proinflammatory cytokine production. Biochemical and molecular dynamic simulation analyses were conducted to examine the properties of the T164S mutant NS1 protein. T164S mutant virus or mutant NS1 was compared to parental wild-type virus or wild-type NS1 in all experiments.

The human PBMCs used in this study were provided by the principal investigator (S.G.V.), senior colleague (J.L.), and coauthor (E.E.O.) and collected in accordance with National University of Singapore Institutional Review Board approval B-12-227. All animal experiments (protocol 2016/SHS/1167) were approved by the Institutional Animal Care and Use Committee of Singapore Health Services and conformed to the National Institutes of Health guidelines and public law.

Cell lines and antibodies

BHK-21 cells [baby hamster kidney fibroblast cells, American Type Culture Collection (ATCC)] were cultured in RPMI 1640 medium (Gibco) supplemented with 10% fetal bovine serum (FBS) and 1% penicillin-streptomycin (P/S) at 37°C in 5% CO₂. C6/36, an *Aedes albopictus* cell line (ATCC), was maintained in RPMI 1640 medium with 10% FBS, 25 mM Hepes, and 1% P/S at 28°C in the absence of CO₂. HuH-7 cells (human hepatocarcinoma cells, ATCC) were cultured in Dulbecco's modified Eagle's medium with 10% FBS, glucose (4.5 g/liter), and 1% P/S at 37°C in 5% CO₂. The preparation and use of mouse 4G2 and humanized 4G2 antibody in this study was previously described (29). Anti-NS1 [56.2; (19)] and NS3 [3F8; (13)] antibodies used in Western blotting (WB) were previously described.

Generation of T164S mutant dengue virus

Full-length DENV2-3295 cDNA clone (GenBank accession number EU081177) used in this study has been previously described (13). Figure 2A shows the schematics of generating the NS1:T164S mutant cDNA infectious clone. RNA was in vitro transcribed from the full-length cDNA clone using T7 mMESSAGE mMACHINE kit (Ambion) and transfected into C6/36 using the previously described electroporation conditions (13). Supernatants from the transfected C6/36 cells were collected on day 7 after transfection (P₀ virus) and passaged once in C6/36 to obtain the P₁ virus stock for infection studies.

In vitro virus replication assay

The in vitro transcribed RNAs of wild type and T164S were transfected into BHK-21 cells as described previously (13) to examine the replication profile of the viruses over the course of 5 days. For infection assay, 1 × 10⁵ HuH-7 cells were infected with DENV2 wild-type or T164S mutant viruses at MOIs of 10 or 1. After 1 hour of incubation at 37°C, virus inocula were removed and replaced with growth medium and sampled as supernatants or TRIzol lysates at indicated time points for plaque, NS1-capture ELISA (26), and viral RNA quantification, respectively, as described in the Supplementary Materials.

Human PBMC infection assay

Human PBMCs were isolated from three healthy donors by Ficoll-Paque (GE Healthcare) extraction method, and 10⁶ PBMCs were infected with either 10⁷ pfu of DENV2 wild-type or T164S mutant virus [presence or absence of 0.05 µg of humanized 4G2 antibody for 2.5 hours at 37°C; (29)]. PBMCs (10⁶) were stimulated with wild-type or T164S sNS1 protein immunoaffinity-purified from infected BHK-21 supernatants for 24 hours (19). Collected supernatants at 24 hours after infection/after stimulation were subjected to IL-6 and TNFα cytokine measurements using Ready-SET-Go! ELISA kits (eBioscience), NS1-capture ELISA (26), and/or standard BHK-21 plaque assay. Cell lysates from the infection assay were harvested at the indicated time points for inflammatory gene profiling using NanoString (see the Supplementary Materials for details).

AG129 mouse infection studies

Sv/129 mice deficient in type I and II IFN receptors (AG129) purchased from B&K Universal (UK) were housed in the biosafety level 2 (BSL-2) animal facility at Duke-NUS, Singapore. All animal experiments were carried out as outlined in an approved protocol. Eight- to 11-week-old female mice were used to examine the in vivo phenotype and pathology induced by T164S mutant virus infection. For the viremic model, mice were inoculated intravenously with 1 × 10⁷ pfu of DENV2

wild-type or T164S mutant virus. Mouse monoclonal 4G2 antibody (50 µg) was administrated intraperitoneally into mice 1 day before infection to induce ADE infection. Blood samples were collected from day 1 to day 6 after infection by submandibular bleeding, and serum samples were subjected to measurements of viral load by real-time RT-PCR and plaque assay, sNS1 by NS1-capture ELISA (26), and cytokines using Ready-SET-Go! ELISA kits (IL-6 and TNFα; eBioscience). Serum complement C3 and MBL2 levels were measured using Mouse Complement C3 and SimpleStep MBL ELISA kits (Abcam).

For lethal infection model, mice preinjected with 50 µg of 4G2 antibody (intraperitoneally) were inoculated intravenously with 1 × 10⁸ pfu of DENV2 wild-type or T164S mutant virus. Mice survival was monitored over the course of 10 days, and mice were sacrificed when they appeared moribund. Serum samples collected on days 1 to 4 after infection were subjected to viremia measurement by real-time RT-PCR. Two to three mice per group (uninfected, DENV2 wild-type, and T164S) were sacrificed on day 3.5 (85 hours after infection) by CO₂ inhalation and perfused with phosphate-buffered saline (PBS) after blood collection from the postcaval vein. Tissues (spleen, liver, and small intestine) were collected and snap-frozen in liquid nitrogen after removal of luminal content from the intestine. These tissues were homogenized in PBS, and the homogenates were subjected to viral load analysis by real-time RT-PCR, proinflammatory IL-6, TNFα, C3, and NS1-capture ELISA (26).

Molecular dynamics simulations

Molecular dynamics simulations using GROMACS 5.1.4 package was performed on the hexameric DENV2 NS1 obtained from the x-ray structure (PDB ID, 4O6B) (11) with in silico mutations introduced according to the DENV2-3295 Singapore strain used in this study. In addition, the T164S mutation was introduced in the mutant hexamer for comparison with the simulations of the wild-type NS1 protein. The details of the simulation parameters can be found in the Supplementary Materials.

Lipid profiling of wild-type and T164S mutant sNS1

The lipid content of the wild-type and T164S mutant hexameric sNS1 was analyzed by LC-MS/MS. Details of the analytics and post-analytics of the lipid profiling can be found in the Supplementary Materials.

Statistical analysis

Statistical analysis was performed using GraphPad Prism v5.0 software. Significance in virus titers measured by plaque assay or RT-PCR and ELISA measurements between the wild-type and T164S virus mutant groups was determined by a nonparametric Mann-Whitney test. Significant differences in the abundance of lipid classes between wild-type virus and T164S mutant virus were compared using an unpaired two-tailed Student *t* test with unequal variance. Comparison of mouse survival rates was performed using the log-rank Mantel-Cox test. Two-way ANOVA with Bonferroni correction was performed to determine significant differences between wild-type and mutant virus groups for kinetics data on mouse viremia and serum complement C3 concentrations. *P* < 0.05 was considered significant. All data were obtained from duplicate of two independent experiments or as otherwise stated.

SUPPLEMENTARY MATERIALS

stm.sciencemag.org/cgi/content/full/11/498/eaat7726/DC1

Materials and Methods

Fig. S1. Genome equivalent (GE), infectivity and plaque morphology of T164S mutant virus.

- Fig. S2. Infectivity of wild-type and T164S mutant virus in the mosquito vector *A. aegypti*.
 Fig. S3. Ex vivo human PBMC infection with wild-type or T164S mutant virus in the absence or presence of humanized 4G2 antibody.
 Fig. S4. Heat map expression profile of inflammation-associated genes after infection of human PBMCs with wild-type or T164S mutant virus.
 Fig. S5. Heat map expression profile of inflammation-associated genes after infection of human PBMCs with wild-type or T164S mutant virus in the presence of humanized 4G2 antibody.
 Fig. S6. Heat map expression profile of clustered inflammation-associated genes after infection of human PBMCs with wild-type or T164S mutant virus.
 Fig. S7. Heat map expression profile of clustered inflammation-associated genes after infection of human PBMCs with wild-type or T164S mutant virus in the presence of humanized 4G2 antibody.
 Fig. S8. Viremia and proinflammatory cytokine production in AG129 mice infected with DENV2 wild-type or T164S mutant virus.
 Fig. S9. Pairwise growth competition assay between wild-type and T164S mutant virus.
 Fig. S10. Proposed mechanism of the increased secretion of the T164S NS1 hexamer.
 Table S1. List of add-on genes in the NanoString Human Inflammation v2 codeset.
 Table S2. Mass spectrometry parameters used for determining the lipid composition of the NS1.
 Table S3. Summary of lipid species and their relative abundance extracted from immunoaffinity-purified wild-type or T164S mutant NS1 proteins.
 Data file S1. Individual-level data for characterization of the T164S mutation in NS1 of dengue virus.
 Data file S2. Individual-level data for infection of human PBMCs ex vivo with wild-type or T164S mutant dengue virus in the absence or presence of humanized 4G2.
 Data file S3. Individual-level data for nonlethal infection of AG129 mice with wild-type or T164S mutant dengue virus.
 Data file S4. Individual-level data for lethal infection of AG129 mice with wild-type or T164S mutant dengue virus.

REFERENCES AND NOTES

- S. Bhatt, P. W. Gething, O. J. Brady, J. P. Messina, A. W. Farlow, C. L. Moyes, J. M. Drake, J. S. Brownstein, A. G. Hoen, O. Sankoh, M. F. Myers, D. B. George, T. Jaenisch, G. R. W. Wint, C. P. Simmons, T. W. Scott, J. J. Farrar, S. I. Hay, The global distribution and burden of dengue. *Nature* **496**, 504–507 (2013).
- R. Rodriguez-Roche, M. Alvarez, T. Gritsun, S. Halstead, G. Kouri, E. A. Gould, M. G. Guzman, Virus evolution during a severe dengue epidemic in Cuba, 1997. *Virology* **334**, 154–159 (2005).
- S. B. Halstead, Intraepidemic increases in dengue disease severity: Applying lessons on surveillance and transmission, in *Clinical Insights in Dengue: Transmission, Diagnosis & Surveillance. The Future Medicine*, J. Whitehorn, Ed. (Future Science Group, London, 2014), pp. 83–101.
- M. Flamand, F. Megret, M. Mathieu, J. Lepault, F. A. Rey, V. Deubel, Dengue virus type 1 nonstructural glycoprotein NS1 is secreted from mammalian cells as a soluble hexamer in a glycosylation-dependent fashion. *J. Virol.* **73**, 6104–6110 (1999).
- I. Gutsche, F. Coulibaly, J. E. Voss, J. Salmon, J. d'Alayer, M. Ermonval, E. Larquet, P. Charneau, T. Krey, F. Megret, E. Guittet, F. A. Rey, M. Flamand, Secreted dengue virus nonstructural protein NS1 is an atypical barrel-shaped high-density lipoprotein. *Proc. Natl. Acad. Sci. U.S.A.* **108**, 8003–8008 (2011).
- D. Watterson, N. Modhiran, P. R. Young, The many faces of the flavivirus NS1 protein offer a multitude of options for inhibitor design. *Antiviral Res.* **130**, 7–18 (2016).
- N. Modhiran, D. Watterson, D. A. Muller, A. K. Panetta, D. P. Sester, L. Liu, D. A. Hume, K. J. Stacey, P. R. Young, Dengue virus NS1 protein activates cells via Toll-like receptor 4 and disrupts endothelial cell monolayer integrity. *Sci. Transl. Med.* **7**, 304ra142 (2015).
- P. R. Beatty, H. Puerta-Guardo, S. S. Killingbeck, D. R. Glasner, K. Hopkins, E. Harris, Dengue virus NS1 triggers endothelial permeability and vascular leak that is prevented by NS1 vaccination. *Sci. Transl. Med.* **7**, 304ra141 (2015).
- P. Avirutnan, N. Punyadee, S. Noisakran, C. Komoltri, S. Thiemmeca, K. Auethavornanan, A. Jairungsri, R. Kanlaya, N. Tangthawornchaikul, C. Puttikhunt, S.-n. Pattanakitsakul, P.-t. Yenchitsomanus, J. Mongkolsapaya, W. Kasirerk, N. Sittisombut, M. Husmann, M. Blettner, S. Vasanawathana, S. Bhakdi, P. Malasit, Vascular leakage in severe dengue virus infections: A potential role for the nonstructural viral protein NS1 and complement. *J. Infect. Dis.* **193**, 1078–1088 (2006).
- B. E. Pickett, E. L. Sadat, Y. Zhang, J. M. Noronha, R. B. Squires, V. Hunt, M. Liu, S. Kumar, S. Zaremba, Z. Gu, L. Zhou, C. N. Larson, J. Dietrich, E. B. Klem, R. H. Scheuermann, ViPR: An open bioinformatics database and analysis resource for virology research. *Nucleic Acids Res.* **40**, D593–D598 (2012).
- D. L. Akey, W. C. Brown, S. Dutta, J. Konwerski, J. Jose, T. J. Jurkiw, J. DelProposto, C. M. Ogata, G. Skiniotis, R. J. Kuhn, J. L. Smith, Flavivirus NS1 structures reveal surfaces for associations with membranes and the immune system. *Science* **343**, 881–885 (2014).
- J. G. H. Low, E.-E. Ooi, T. Tolvenstam, Y.-S. Leo, M. L. Hibberd, L.-C. Ng, Y.-L. Lai, G. S. L. Yap, C. S. C. Li, S. G. Vasudevan, A. Ong, Early dengue infection and outcome study (EDEN)—Study design and preliminary findings. *Ann. Acad. Med. Singapore* **35**, 783–789 (2006).
- M. Y. F. Tay, W. G. Saw, Y. Zhao, K. W. K. Chan, D. Singh, Y. Chong, J. K. Forwood, E. E. Ooi, G. Grüber, J. Lescar, D. Luo, S. G. Vasudevan, The C-terminal 50 amino acid residues of dengue NS3 protein are important for NS3-NS5 interaction and viral replication. *J. Biol. Chem.* **290**, 2379–2394 (2015).
- J. Pompon, M. Manuel, G. K. Ng, B. Wong, C. Shan, G. Manokaran, R. Soto-Acosta, S. S. Bradrick, E. E. Ooi, D. Missé, P.-Y. Shi, M. A. Garcia-Blanco, Dengue subgenomic flaviviral RNA disrupts immunity in mosquito salivary glands to increase virus transmission. *PLOS Pathog.* **13**, e1006535 (2017).
- M. J. Conway, T. M. Colpitts, E. Fikrig, Role of the vector in arbovirus transmission. *Annu. Rev. Virol.* **1**, 71–88 (2014).
- M. G. Guzman, E. Harris, Dengue. *Lancet* **385**, 453–465 (2015).
- P. N. Paradkar, E. E. Ooi, B. J. Hanson, D. J. Gubler, S. G. Vasudevan, Unfolded protein response (UPR) gene expression during antibody-dependent enhanced infection of cultured monocytes correlates with dengue disease severity. *Biosci. Rep.* **31**, 221–230 (2011).
- B. E. E. Martina, P. Koraka, A. D. M. E. Osterhaus, Dengue virus pathogenesis: An integrated view. *Clin. Microbiol. Rev.* **22**, 564–581 (2009).
- K. Rozen-Gagnon, N. J. Moreland, C. Ruedl, S. G. Vasudevan, Expression and immunoaffinity purification of recombinant dengue virus 2 NS1 protein as a cleavable SUMOstar fusion. *Protein Expr. Purif.* **82**, 20–25 (2012).
- W. Xu, N. V. Solis, S. G. Filler, A. P. Mitchell, Pathogen gene expression profiling during infection using a nanostring nCounter platform. *Methods Mol. Biol.* **1361**, 57–65 (2016).
- G. Manokaran, E. Finol, C. Wang, J. Gunaratne, J. Bahl, E. Z. Ong, H. C. Tan, O. M. Sessions, A. M. Ward, D. J. Gubler, E. Harris, M. A. Garcia-Blanco, E. E. Ooi, Dengue subgenomic RNA binds TRIM25 to inhibit interferon expression for epidemiological fitness. *Science* **350**, 217–221 (2015).
- J. Fink, F. Gu, L. Ling, T. Tolvenstam, F. Olfat, K. C. Chin, P. Aw, J. George, V. A. Kuznetsov, M. Schreiber, S. G. Vasudevan, M. L. Hibberd, Host gene expression profiling of dengue virus infection in cell lines and patients. *PLOS Negl. Trop. Dis.* **1**, e86 (2007).
- H. T. Long, M. L. Hibberd, T. T. Hien, N. M. Dung, T. Van Ngoc, J. Farrar, B. Wills, C. P. Simmons, Patterns of gene transcript abundance in the blood of children with severe or uncomplicated dengue highlight differences in disease evolution and host response to dengue virus infection. *J. Infect. Dis.* **199**, 537–546 (2009).
- J. Chen, M. M.-L. Ng, J. J. H. C. Chu, Activation of TLR2 and TLR6 by dengue NS1 protein and its implications in the immunopathogenesis of dengue virus infection. *PLOS Pathog.* **11**, e1005053 (2015).
- D. A. Muller, P. R. Young, The flavivirus NS1 protein: Molecular and structural biology, immunology, role in pathogenesis and application as a diagnostic biomarker. *Antiviral Res.* **98**, 192–208 (2013).
- S. Watanabe, K. H. Tan, A. P. S. Rathore, K. Rozen-Gagnon, W. Shuai, C. Ruedl, S. G. Vasudevan, The magnitude of dengue virus NS1 protein secretion is strain dependent and does not correlate with severe pathologies in the mouse infection model. *J. Virol.* **86**, 5508–5514 (2012).
- A.-M. Chacko, S. Watanabe, K. J. Herr, S. Kalimuddin, J. Y. Tham, J. Ong, M. Reolo, R. M. F. Serrano, Y. B. Cheung, J. G. H. Low, S. G. Vasudevan, ¹⁸F-FDG as an inflammation biomarker for imaging dengue virus infection and treatment response. *JCI Insight* **2**, 93474 (2017).
- R. M. Zellweger, T. R. Prestwood, S. Shresta, Enhanced infection of liver sinusoidal endothelial cells in a mouse model of antibody-induced severe dengue disease. *Cell Host Microbe* **7**, 128–139 (2010).
- S. Watanabe, K. W. K. Chan, J. Wang, L. Rivino, S.-M. Lok, S. G. Vasudevan, Dengue virus infection with highly-neutralizing levels of cross-reactive antibodies causes acute lethal small intestinal pathology without a high level of viremia in mice. *J. Virol.* **89**, 5847–5861 (2015).
- M. H. de Bruijn, G. H. Fey, Human complement component C3: cDNA coding sequence and derived primary structure. *Proc. Natl. Acad. Sci. U.S.A.* **82**, 708–712 (1985).
- M. Ohainle, A. Balmaseda, A. R. Macalalad, Y. Tellez, M. C. Zody, S. Saborio, A. Nuñez, N. J. Lennon, B. W. Birren, A. Gordon, M. R. Henn, E. Harris, Dynamics of dengue disease severity determined by the interplay between viral genetics and serotype-specific immunity. *Sci. Transl. Med.* **3**, 114ra128 (2011).
- K. C. Leitmeyer, D. W. Vaughn, D. M. Watts, R. Salas, I. Villalobos, C. de, C. Ramos, R. Rico-Hesse, Dengue virus structural differences that correlate with pathogenesis. *J. Virol.* **73**, 4738–4747 (1999).
- J. Liu, Y. Liu, K. Nie, S. Du, J. Qiu, X. Pang, P. Wang, G. Cheng, Flavivirus NS1 protein in infected host sera enhances viral acquisition by mosquitoes. *Nat. Microbiol.* **1**, 16087 (2016).
- P. Avirutnan, R. E. Hauhart, M. A. Marovich, P. Garred, J. P. Atkinson, M. S. Diamond, Complement-mediated neutralization of dengue virus requires mannose-binding lectin. *MBio* **2**, e00276-11 (2011).

35. E. Navarro-Sánchez, P. Després, L. Cedillo-Barrón, Innate immune responses to dengue virus. *Arch. Med. Res.* **36**, 425–435 (2005).
36. C. A. Quiner, P. Parameswaran, A. T. Ciota, D. J. Ehrbar, B. L. Dodson, S. Schlesinger, L. D. Kramer, E. Harris, Increased replicative fitness of a dengue virus 2 clade in native mosquitoes: Potential contribution to a clade replacement event in Nicaragua. *J. Virol.* **88**, 13125–13134 (2014).
37. P. W. Mason, Maturation of Japanese encephalitis virus glycoproteins produced by infected mammalian and mosquito cells. *Virology* **169**, 354–364 (1989).
38. P. Scaturro, M. Cortese, L. Chatel-Chaix, W. Fischl, R. Bartenschlager, Dengue virus non-structural protein 1 modulates infectious particle production via interaction with the structural proteins. *PLOS Pathog.* **11**, e1005277 (2015).
39. L. B. Tanner, C. Chng, X. L. Guan, Z. Lei, S. G. Rozen, M. R. Wenk, Lipidomics identifies a requirement for peroxisomal function during influenza virus replication. *J. Lipid Res.* **55**, 1357–1365 (2014).
40. N. Menzel, W. Fischl, K. Hueging, D. Bankwitz, A. Frentzen, S. Haid, J. Gentzsch, L. Kaderali, R. Bartenschlager, T. Pietschmann, MAP-kinase regulated cytosolic phospholipase A2 activity is essential for production of infectious hepatitis C virus particles. *PLOS Pathog.* **8**, e1002829 (2012).
41. K. W. K. Chan, S. Watanabe, R. Kavishna, S. Alonso, S. G. Vasudevan, Animal models for studying dengue pathogenesis and therapy. *Antiviral Res.* **123**, 5–14 (2015).
42. Y. Liu, J. Liu, S. Du, C. Shan, K. Nie, R. Zhang, X.-F. Li, R. Zhang, T. Wang, C.-F. Qin, P. Wang, P.-Y. Shi, G. Cheng, Evolutionary enhancement of Zika virus infectivity in *Aedes aegypti* mosquitoes. *Nature* **545**, 482–486 (2017).
43. P. Shannon, A. Markiel, O. Ozier, N. S. Baliga, J. T. Wang, D. Ramage, N. Amin, B. Schwikowski, T. Ideker, Cytoscape: A software environment for integrated models of biomolecular interaction networks. *Genome Res.* **13**, 2498–2504 (2003).

Acknowledgments: We thank E. Leman for editorial assistance and M. Diamond, A. Bertoletti, M. G. Blanco, Y. B. Cheung, J. Low, and C. Swarbrick for valuable discussions. We also thank S. Albani, C. J. H. Chua, and S. N. Hazirah for access to the NanoString Technology platform and M. C. Manuel for providing technical training and assistance in rearing *A. aegypti*. We acknowledge the Advanced Bioimaging Core of Duke-NUS Singapore Health Services for the

scientific and technical assistance with confocal microscopy. We thank the National Supercomputing Centre Singapore (<http://www.nscc.sg>) for computational resources provided for molecular dynamics simulations. **Funding:** Supported by National Medical Research Council of Singapore grants NMRC/CBRG/2016 (S.G.V.), NMRC/CBRG/0065/2014 (S.A.), NMRC/CIRG/1374/2013 (E.E.O.), and NMRC/ZRRF/007/2017 (J.P.); National Research Foundation grant NRF2015-05 (M.R.W.); and Ministry of Education in Singapore MOE ACRF Tier 3 Grant Number MOE2012-T3-1-008 (P.J.B.). **Author contributions:** K.W.K.C., S.W., S.B.H., and S.G.V. conceived the study. K.W.K.C. performed and analyzed the *in vitro* infection studies in cell lines and human PBMCs. K.W.K.C., J.Y.J., and J.P. performed and analyzed the mosquito infection studies. K.W.K.C. and S.W. performed and analyzed the *in vivo* mouse studies. The phylogenetic analysis was conducted by K.W.K.C., D.T., and D.V. The molecular dynamics simulation analysis was carried out by J.K.M. and P.J.B. The lipid profiling was carried out and analyzed by K.W.K.C., B.B., F.T., M.R.W., S.A., and E.E.O. provided plasmid reagents and analyzed the *in vitro* infection studies; K.W.K.C. and S.G.V. wrote the manuscript. All authors read and commented on the final manuscript. **Competing interests:** S.B.H. has received support from GlaxoSmithKline, Sanofi Pasteur, Merck, and Takeda. E.E.O. is an Advisory Board member for Sanofi Pasteur, Janssen Pharmaceuticals, and Takeda. S.G.V. has received support from Janssen Pharmaceuticals for the testing of antiviral drugs. **Data and materials availability:** All data associated with this study are present in the paper or the Supplementary Materials. The engineered T164S mutant dengue virus is available from S.G.V. through a material transfer agreement.

Submitted 3 April 2018
Resubmitted 11 October 2018
Accepted 3 December 2018
Published 26 June 2019
10.1126/scitranslmed.aat7726

Citation: K. W. K. Chan, S. Watanabe, J. Y. Jin, J. Pompon, D. Teng, S. Alonso, D. Vijaykrishna, S. B. Halstead, J. K. Marzinek, P. J. Bond, B. Burla, F. Torta, M. R. Wenk, E. E. Ooi, S. G. Vasudevan, A T164S mutation in the dengue virus NS1 protein is associated with greater disease severity in mice. *Sci. Transl. Med.* **11**, eaat7726 (2019).

Science Translational Medicine

A T164S mutation in the dengue virus NS1 protein is associated with greater disease severity in mice

Kitti Wing Ki Chan, Satoru Watanabe, Jocelyn Y. Jin, Julien Pompon, Don Teng, Sylvie Alonso, Dhanasekaran Vijaykrishna, Scott B. Halstead, Jan K. Marzinek, Peter J. Bond, Bo Burla, Federico Torta, Markus R. Wenk, Eng Eong Ooi and Subhash G. Vasudevan

Sci Transl Med 11, eaat7726.
DOI: 10.1126/scitranslmed.aat7726

Molecular insights into dengue virus NS1

Several hundred thousand cases of severe dengue disease occur annually worldwide. Using phylogenetic analysis of publicly available dengue virus sequences, Chan *et al.* now show that the T164S mutation in the dengue virus NS1 protein correlated with severe dengue epidemics in the Americas. The investigators reverse engineered this mutation into the NS1 protein of a dengue virus serotype 2 mildly infectious strain. The resulting T164S mutant dengue virus produced more secreted NS1 than wild-type virus in infected mammalian cell lines, mosquitoes, and mice. Gene expression analysis and direct measurement of factors promoting disease severity in mice revealed an association between the T164S mutation in NS1 and its lipoprotein structure.

ARTICLE TOOLS

<http://stm.scienmag.org/content/11/498/eaat7726>

SUPPLEMENTARY MATERIALS

<http://stm.scienmag.org/content/suppl/2019/06/24/11.498.eaat7726.DC1>

RELATED CONTENT

<http://stm.scienmag.org/content/scitransmed/9/409/eaan1589.full>
<http://stm.scienmag.org/content/scitransmed/9/405/eaal5088.full>
<http://stm.scienmag.org/content/scitransmed/7/304/304ra141.full>

REFERENCES

This article cites 42 articles, 18 of which you can access for free
<http://stm.scienmag.org/content/11/498/eaat7726#BIBL>

PERMISSIONS

<http://www.scienmag.org/help/reprints-and-permissions>

Use of this article is subject to the [Terms of Service](#)

Science Translational Medicine (ISSN 1946-6242) is published by the American Association for the Advancement of Science, 1200 New York Avenue NW, Washington, DC 20005. 2017 © The Authors, some rights reserved; exclusive licensee American Association for the Advancement of Science. No claim to original U.S. Government Works. The title *Science Translational Medicine* is a registered trademark of AAAS.